JTTEE5 9:264-273

Microstructural Characterization of Radio Frequency and Direct Current Plasma-Sprayed Al_2O_3 Coatings

H.C. Chen, E. Pfender, B. Dzur, and G. Nutsch

(Submitted 31 March 1999; in revised form 7 December 1999)

Microstructures of radio frequency (RF) and direct current (DC) plasma-sprayed Al_2O_3 coatings deposited onto steel substrates were characterized using scanning electron microscopy (SEM), X-ray diffraction (XRD), electron microprobe analysis (EMPA), polarizing optical microscopy (OM), and transmission electron microscopy (TEM). Because RF and DC plasmas produce different particle heating and acceleration, the morphology, phase structure, and fracture modes of the coatings vary substantially. In the case of RF coatings, a clear lamellar microstructure with relatively thick lamellae was observed, which is due to the large particles and the low particle velocities, with α-Al_2O_3 as the predominant phase and with delamination type of fracture detected on the fracture surface. In contrast, the DC coatings consisted of predominantly metastable γ-Al_2O_3 as well as amorphous phases, with a mixed fracture mode of the coating observed. In spite of limited interfacial interdiffusion detected by EMPA, TEM showed an interfacial layer existing at the interface between the coating and the substrate for both cases. For RF coatings, the interfacial layer on the order of 1 μm was composed of three sublayers, each of which was different in composition and morphology. However, the interfacial layer for the DC coating consisted primarily of an amorphous phase, containing both coating and substrate materials with or without platelike microcrystals; although in some regions a thick amorphous Al_2O_3 layer was in direct contact with the substrate.

Keywords alumina coatings, microstructure, interface, RF and DC plasma spraying

1. Introduction

Direct current (DC) plasma spraying has been around for many years; it is known as an economic way to produce all kinds of coatings for a variety of applications. In recent years, there has been a growing interest in using radio frequency (RF) plasmas for making coatings. Such plasmas are also designated as inductively coupled plasmas (ICP) in the following. Both plasma spray methods have been applied for spheroidization of powders, for preparation of solid oxide fuel cell electrodes,[1] and for other applications. Compared to DC plasmas, RF plasmas provide more uniform plasma temperature and velocity distributions as well as longer dwell time of particles in the plasma due to the lower plasma velocities. This fact allows injection of larger particles. In addition, since particle deformation coupled with freezing of molten particles produces splats that are different in both cases, it is expected that the RF and DC coatings will have different microstructures and, therefore, different properties.

Many studies have been concerned with differences of the molten particle impact on coating formation,[2] on properties of the plasma jet,[3] and on in-flight particle behavior[4] for both cases. Recently, studies have been reported on characterization of plasma-sprayed coatings by transmission electron microscopy (TEM), considering thermal barrier coatings (TBCs),[5,6] alumina coatings,[7] and Ni-Al coatings.[8] There have been, however, no detailed studies reported on microstructural differences between the coatings prepared by RF and DC plasma spraying. In this paper, X-ray diffraction (XRD), scanning electron microscopy (SEM), TEM, polarizing optical microscopy (OM), and four-point bending fracture studies have been used to investigate the microstructures of the RF and DC coatings.

H.C. Chen, Department of Mechanical Engineering, University of Minnesota, is now with Praxair, Inc., Tonawanda, NY 14151; **E. Pfender,** Department of Mechanical Engineering, University of Minnesota, Minneapolis, MN 55455; and **B. Dzur** and **G. Nutsch,** Technical University of Ilmenau, Ilmenau, Germany.

2. Experimental Materials and Methods

Commercial alumina powder, −45 to 22 μm (Sulzer Metco, Westbury, NY), was used for preparation of DC plasma-sprayed coatings. The substrate was 100 mm long, 50 mm wide, and 5 mm thick consisting of mild steel, which was ultrasonically cleaned and grit blasted with 60 mesh Al_2O_3 sand under pressures of around 0.4 MPa for approximately 30 s. The substrate was attached to a rotating 305 mm diameter disk and repeatedly traversed through the plasma jet with a velocity of 0.56 ms^{-1}. Coatings 0.4 mm thick were formed using a Praxair SG-100 (Appleton, WI) plasma spray torch, which was operated in the subsonic mode (anode 2083-730, cathode 1083A-720, and gas injector 2083-112). The spray powder, suspended in an argon carrier gas, was injected through the internal powder feed port (located about 10 mm upstream of the torch exit) with a velocity of about 7 ms^{-1}. The DC plasma spraying conditions for this experiment are summarized in Table 1.

The laboratory-manufactured RF plasma spray torch (University of Ilmenau, Ilmenau, Germany), which consisted of a 27 mm i.d. quartz tube surrounded by a six-turn induction coil

Table 1 DC plasma spraying conditions

Parameters	Settings
Arc current	850 A
Arc gas flow rate	Ar, 50 slm; He, 16 slm
Carrier gas flow rate	Ar, 4.5 slm
Powder feed rate	25 g/min
Standoff distance	70 mm
Substrate velocity	0.56 ms^{-1}
Torch nozzle i.d.	8 mm
Powder injector i.d.	2 mm

Table 2 RF plasma spraying conditions

Parameters	Settings
Plasma gas flow rate	Ar, 6.7 slm
Sheath gas flow rate	Ar, 33.3 slm; N_2, 75 slm
Carrier gas flow rate	Ar, 2 slm
Plate power	12 kW
Standoff distance	175 mm
Powder feed rate	3.0 g/min

connected to the power supply, was used for preparation of RF plasma-sprayed coatings. It was operated at 4 MHz at a plate power of 12 kW producing atmospheric pressure plasma. The commercial alumina powder, 80 to 100 μm in size (Sulzer Metco), suspended in an argon gas, was injected into the plasma jet through a water-cooled stainless steel probe with its orifice located at the beginning of the second turn of the inductor. The conditions for this experiment are summarized in Table 2.

The XRD method was used to identify the phase structure in both the DC and RF coatings. The X-ray system, a Siemens D-500 diffractometer (Siemens AG, Munich), was operated through a microcomputer using several specialized software packages such as SEARCH/MATCH (Siemens AG) with JCPDS cards. The radiation source used was monochromatic CuK_α generated at 45 kV and 40 mA.

The specimens for metallographic examination were first impregnated with epoxy resin under vacuum, cut perpendicular to the coating surface with a low speed saw, and polished with a Struer's (Westlake, OH) grind/polish system. Microstructure, composition profiles, and X-ray maps were analyzed for cross-sectional coatings using a polarizing OM and a computerized JEOL JXA 8900 Superprobe (Japan Electron Optics Ltd., Tokyo).

The fracture surface morphologies of the cross-sectional coating for both cases were analyzed by a JEOL 840 scanning electron microscope after controlled fracture of the coating-substrate system. A slot 1 mm wide and 4.5 mm deep was cut into the middle of the sample from the rear side. The sample (50 mm length, 4 mm width, 5 mm height) so prepared was then placed in two special fixtures in order to carry out the bending test with a MTS machine. The sample was subjected to four-point bending (innerspan/outerspan: 1/2) with a displacement rate of 0.1 mm per min. Using this bending test, the sample was fractured on the front side, with the coating remaining attached to the substrate after fracture.

Techniques for preparation of TEM cross-sectional samples of the coating-substrate interface used the following procedures. Two samples were first glued together face-to-face with epoxy and then a thin slice 1 mm thick was sectioned off along the direction normal to the coating surface. The slice was then attached to a tripod polisher with glue, thinned mechanically, and polished from both sides until the ceramic coating became transparent. Finally, the sample thickness was further reduced with a low-angle ion-thinning Precise Ion Polishing System (PIPS). The samples containing the coating-substrate interfaces were examined and analyzed using the Philips EM-30 transmission electron microscope (Philips Electronic Instruments Corp., Mahwah, NJ), equipped with a qualitative microanalysis unit.

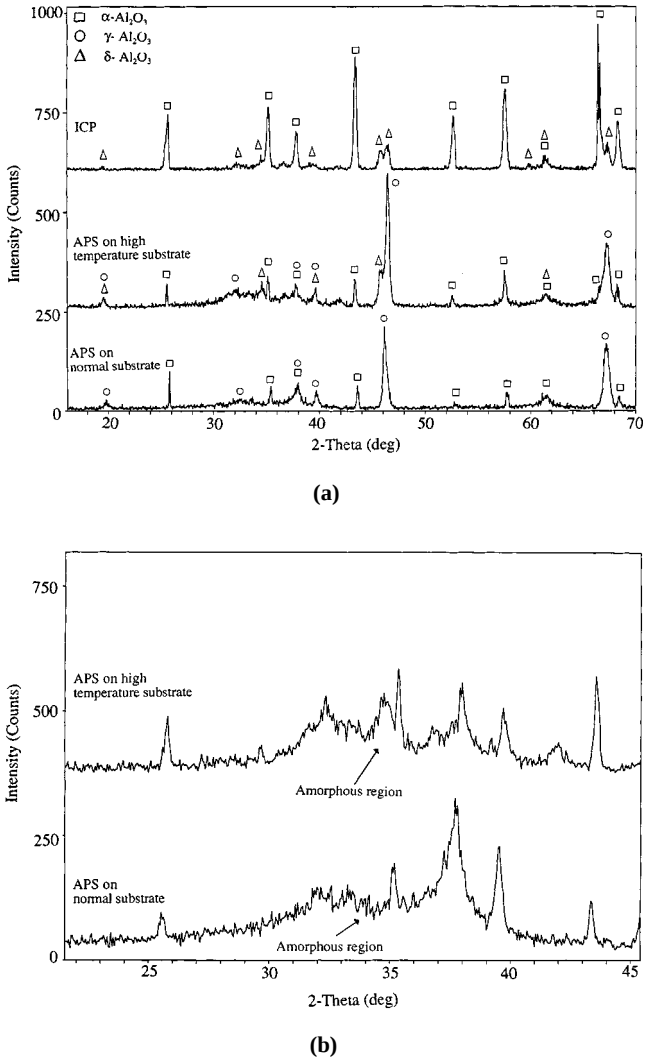

Fig. 1 XRD profiles of RF and DC coatings: (**a**) normal scan speed of XRD and (**b**) slow scan speed of XRD.

3. Experimental Results and Analysis

3.1 Phase Compositions and Distributions of DC and RF Coatings

The XRD analysis showed that phase composition of the coating depends mostly on substrate temperature (cooling rate) and the process used to prepare the coating. In the case of DC plasma spraying with typical substrate temperatures of less

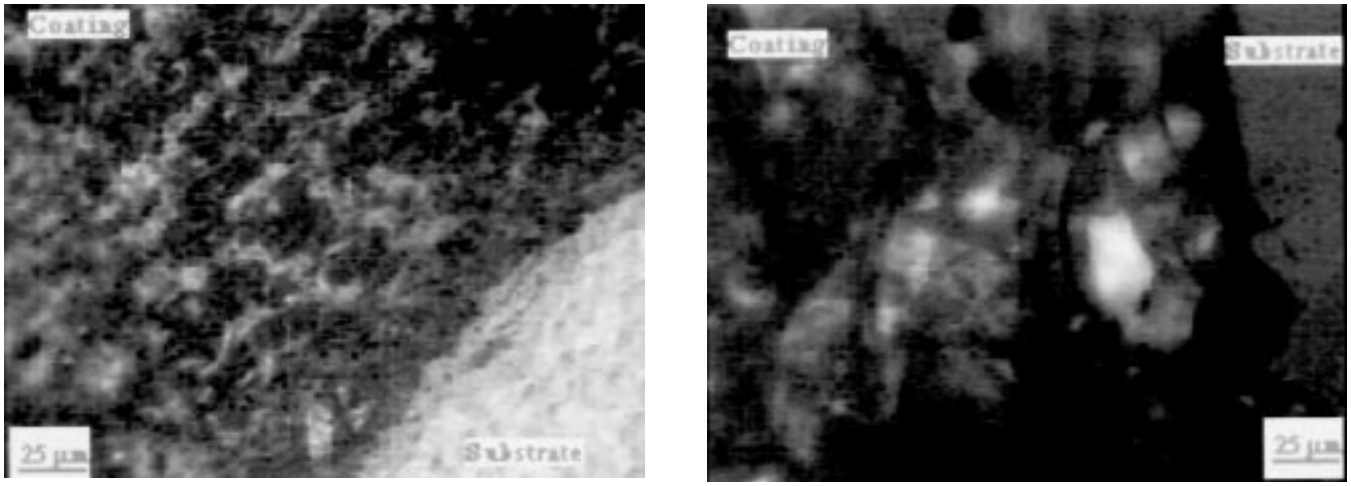

(a) **(b)**

Fig. 2 Optical microscopic images of DC and RF coatings under polarizing conditions: (**a**) DC coating and (**b**) RF coating

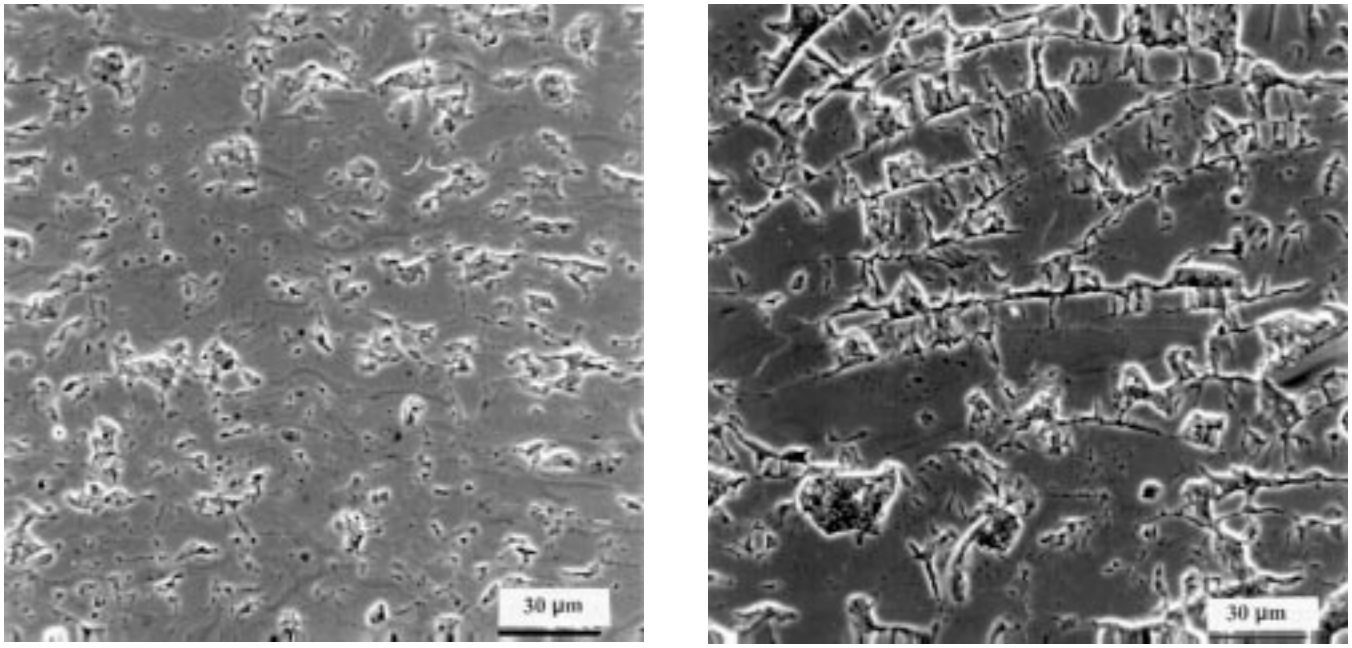

(a) **(b)**

Fig. 3 SEM micrographs of cross-sectional DC and RF coatings: (**a**) DC coating and (**b**) RF coating

than 300 °C, the coating was composed of metastable γ-Al_2O_3 and α-Al_2O_3, as well as of amorphous phases, with γ-Al_2O_3 as the predominant phase, as shown in Fig. 1(a). With high substrate temperatures (higher than 500 °C), δ-Al_2O_3 was found in the coating due to transformation of γ into δ after cooling down of the coating. It should be pointed out that the amorphous phase existed in the coating even at high substrate temperatures (Fig. 1b). This is probably due to high cooling rates typical for the deposition. In the amorphous region, several peaks were found, which related to partial crystallization of the amorphous phase. In the case of the RF plasma spraying process, the coating consisted of α-Al_2O_3 and δ-Al_2O_3, with the stable α-Al_2O_3 as the predominant phase.

Because α, γ, and δ phases of Al_2O_3 material have different symmetries in their crystal structures, each of them can be made visible by using polarizing light at certain incident angles. Figure 2(a) shows such a polarizing OM image, indicating the existence of α phase (bright regions) across the entire cross-section of the DC coating. The α phase, amounting to 20 to 30% in volume, distributes uniformly parallel to the coating surface. The δ phase (bright regions in Fig. 2b) in the RF coating, on the other hand, contributes less than 5% in volume and exists inside large lamellae.

Figure 3 shows SEM micrographs of cross-sectional RF and DC coatings. Unlike DC coatings (Fig. 3a), RF coatings (Fig. 3b) show thicker lamellae and a more porous structure, which is be-

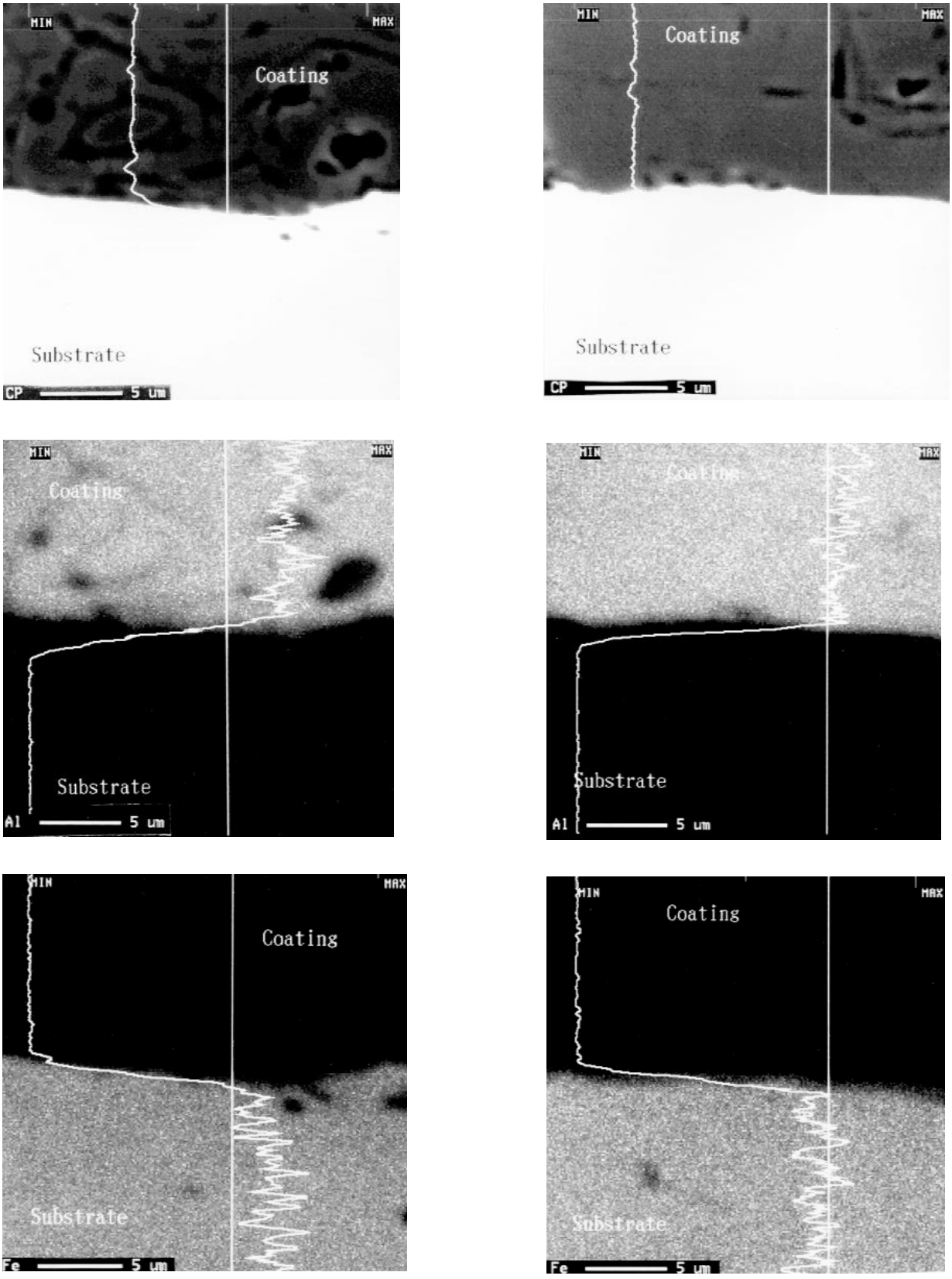

(a) **(b)**

Fig. 4 X-ray maps and profiles of Fe and Al in the coating-substrate interfacial region: (**a**) DC coating, (**b**) RF coating

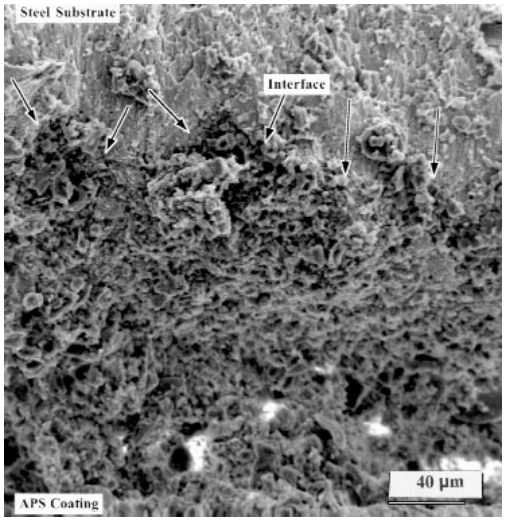

(a)

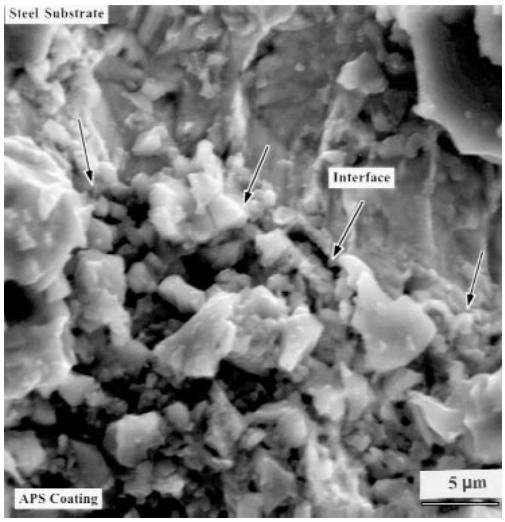

(b)

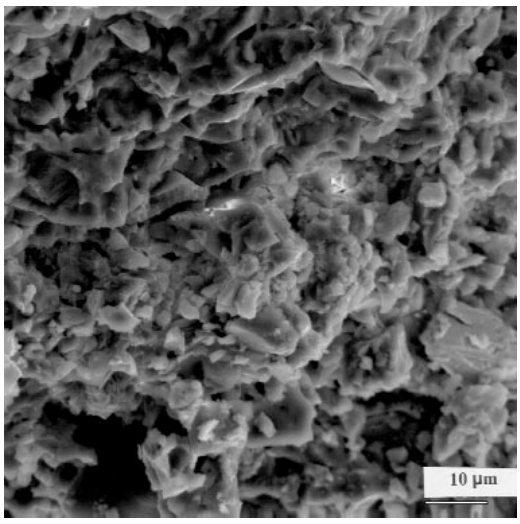

(c)

Fig. 5 Fracture surfaces of DC coating under four-point bending, SEM: (**a**) close to the substrate, (**b**) high magnification of (**a**), and (**c**) away from the substrate

lieved to be caused by the relatively large particles used and low particle velocities involved in the process.

3.2 Composition Distributions in the Interfacial Region

Composition distributions of elements were carried out on polished cross-sections using a computerized superprobe. Figure 4 shows X-ray maps and profiles of Fe and Al in the interfacial regions between the coating and the substrate for both cases. Although limited interdiffusion between Al and Fe was detected, the profiles of Fig. 4 show a mixed zone of Al and Fe existing in the interfacial region of the RF or DC sprayed coatings. The thickness of the mixed zone for both cases is on the order of 1 μm.

3.3 Fractography

In order to analyze the bonding between the coating and the substrate and between the splats within the coating, the DC and

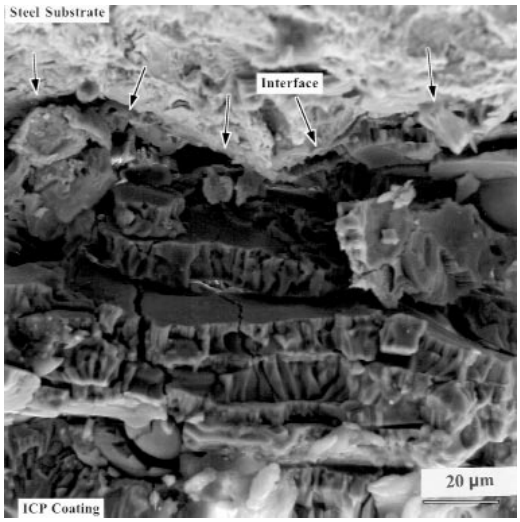

(a)

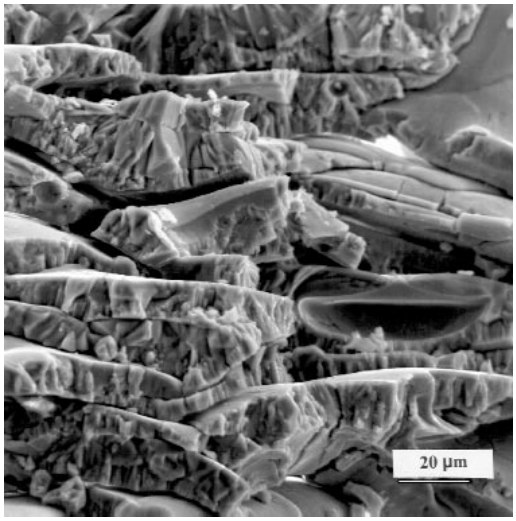

(b)

Fig. 6 Fracture surfaces of RF coating under four-point bending, SEM: (**a**) close to the substrate and (**b**) away from the substrate

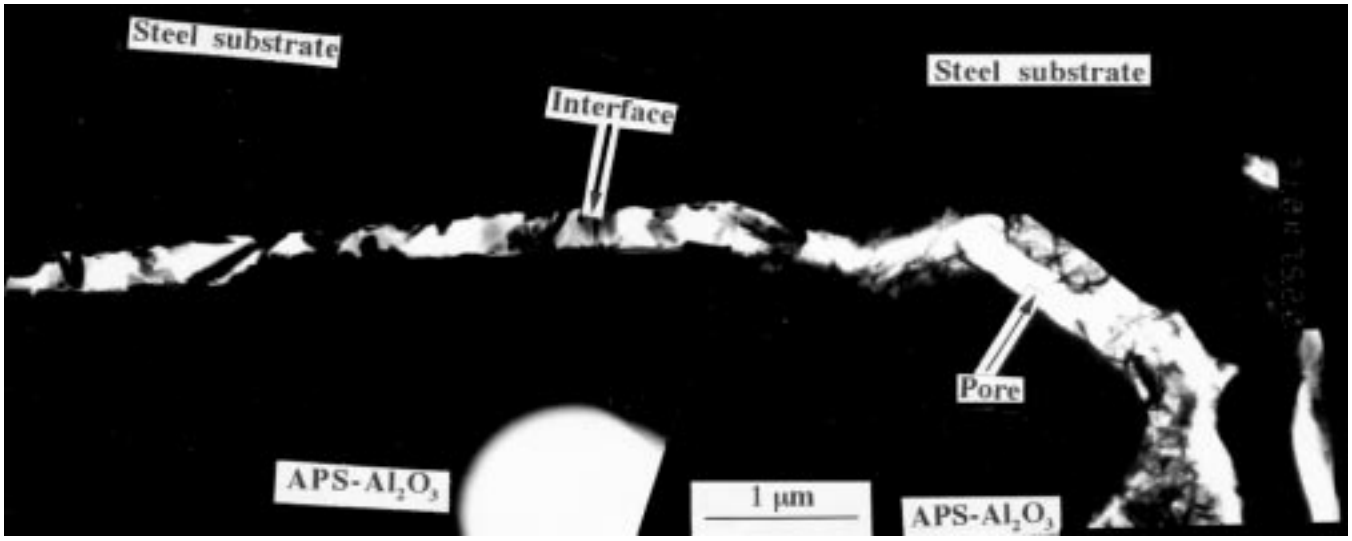

(a)

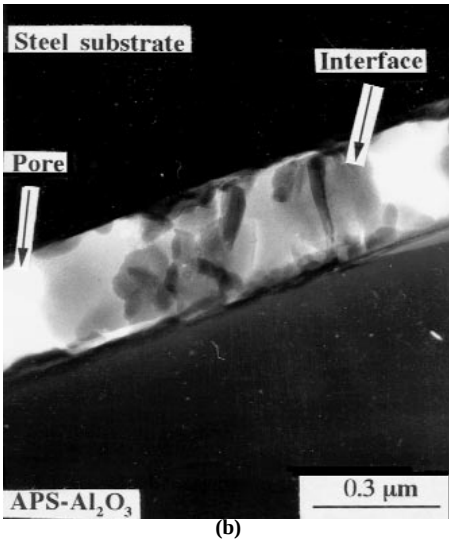

(b)

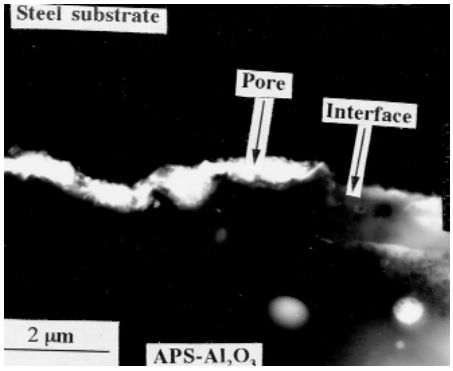

(c)

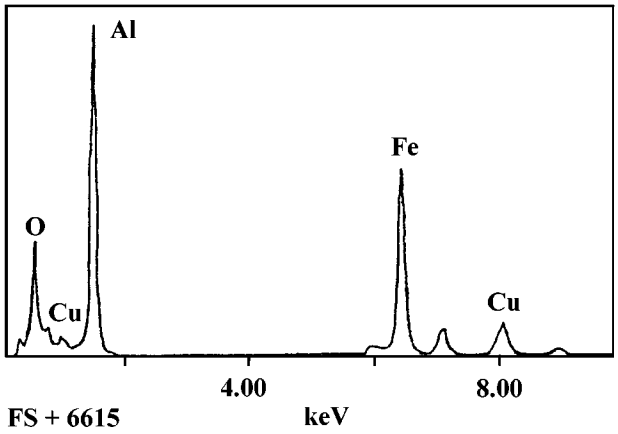

(d)

Fig. 7 TEM micrographs of the interfacial layer between the DC coating and the substrate: (**a**) morphology of interfacial layer. (**b**) interfacial region showing platelike microcrystals grown in the amorphous matrix (**c**) interfacial region showing only an amorphous phase, and (**d**) EDS of the interfacial layer

RF coatings were fractured using the previously described four-point bending process. Figure 5 shows SEM micrographs of fracture surfaces of the DC coatings. As shown in these figures, in the area close to the substrate, the coating was composed of fine grains of different sizes and was bonded well with the substrate (Fig. 5a), with no cracks detected along the interface (Fig. 5b). The fracture in this region was a quasi-cleavage type of fracture, with tearing ridges visible on the fracture surface. In the area away from the substrate, the fracture was a mixed mode of quasi-cleavage and delamination type of fracture (Fig. 5c). In this region of the coating, the lamellar structure is not obvious. Figure 6 shows a clear lamellar structure on the fracture surfaces of the RF coating in the area close to (Fig. 6a) and away from (Fig. 6b) the substrate. As seen in these figures, the coating shows delamination type of fracture with columnar grains visible inside the lamellae and with stretched pores and microcracks along the lamellae. This suggests that the lamellae were bonded together by mechanical interlocking. In the area close to the substrate, unlike in the case of the DC coating, there are no fine or equiaxed grains on the fracture sur-

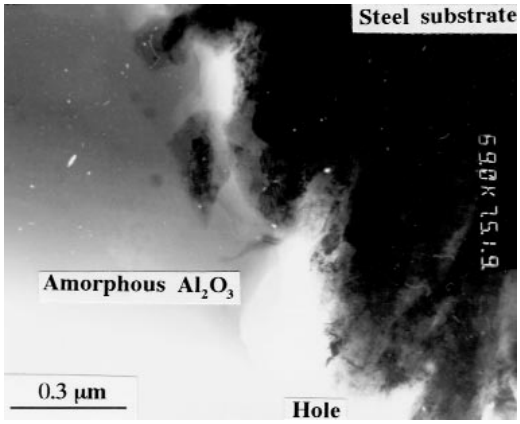

(a)

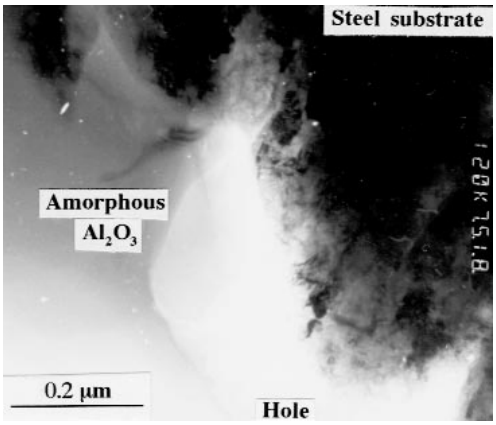

(b)

Fig. 8 TEM micrographs showing no interfacial layer in the DC coating: (**a**) amorphous Al_2O_3 coating directly contacted with the substrate and (**b**) higher magnification of (**a**)

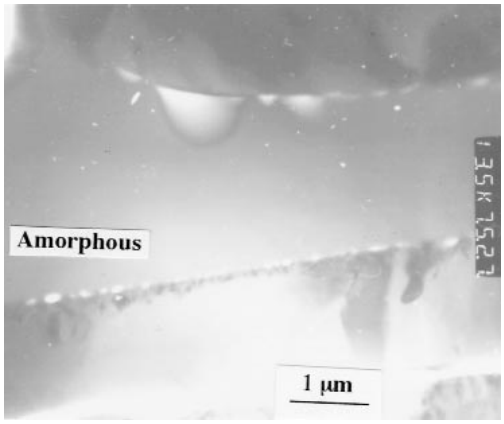

(a)

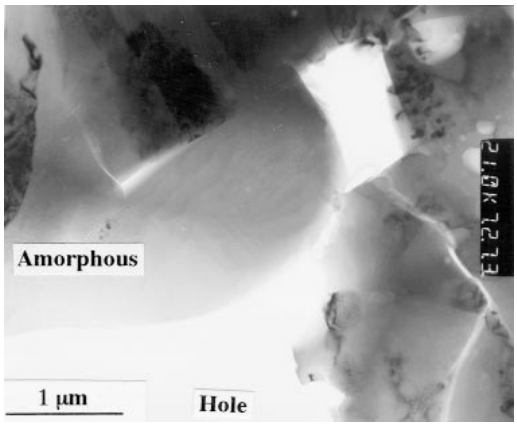

(b)

Fig. 9 Amorphous Al_2O_3 phase existing in the DC coating, TEM: (**a**) between lamellae and (**b**) in the corner between the lamellae

face. In addition, microcracks are also visible along the interface between the coating and the substrate. In summary, the features of the fracture surfaces are different from those observed in the DC coatings. These differences are attributed to the larger particles used and lower velocities characteristic for RF plasma spraying.

3.4 TEM Observation of Coating-Substrate Interface

The samples prepared in this study allow a direct observation of the interfacial region between the coating and the substrate by TEM. The following results show that the microstructures of RF and DC coatings are different not only on the fracture surfaces, but also in the TEM observed interfacial region.

DC coating/substrate interface. The TEM observations show that DC plasma-sprayed coatings were not mechanically separated from the substrate. An interfacial layer, less than 1 μm thick and amorphous in nature identified by selected area electron diffraction (SAED), existed between the coating and the substrate, as shown in Fig. 7(a). The pores in the interfacial layer may be due to preferential erosion during the ion-milling process (the same applies to Figs. 8 and 10). Under higher magnification, TEM shows that the interface exhibits two different morphologies. In most regions along the interfacial line, the interfacial layer consists of an amorphous phase and platelike microcrystals, as shown in Fig. 7(b). Only in some regions was the interfacial layer composed entirely of amorphous phase (Fig. 7c). Energy-dispersive spectroscopy (EDS) qualitative microanalysis conducted simultaneously with TEM observations revealed that the interfacial layer contained both the coating and substrate materials (Fig. 7d), which is believed to be a consequence of the plasma spraying process.[5] Specifically, in some small regions, TEM did not reveal an interfacial layer between the coating and the substrate; only a relatively thick layer of amorphous Al_2O_3 was in direct contact with the substrate, as shown in Fig. 8. This is due to the strong quenching effect of the molten Al_2O_3 particles upon impact on the cold substrate.

Transmission electron microscopy also shows large amounts of amorphous Al_2O_3 between the lamellae and in the corner area where lamellae meet, as shown in Fig. 9. This result is consistent with XRD analysis (Fig. 1b). In addition, due to high resolution, TEM reveals columnar grains well-grown within the lamellae (Fig. 10a) and α phase embedded in the γ matrix (Fig. 10b).

RF coating/substrate interface. The TEM analysis found that the coating/substrate interface in the case of RF-sprayed coatings was much different from the one produced by DC spraying. Instead of being amorphous in nature, the interface

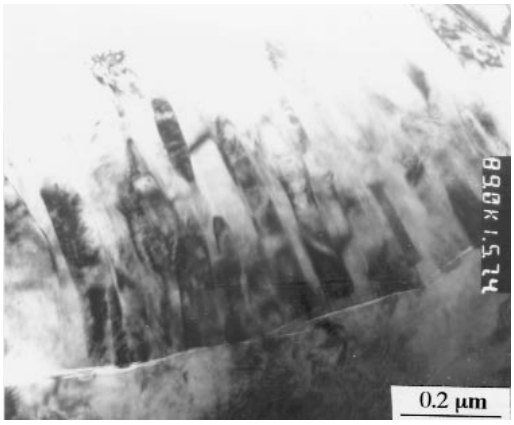

(a)

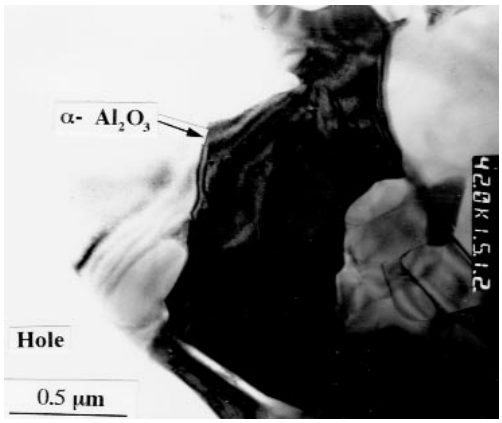

(b)

Fig. 10 TEM micrographs showing (**a**) columnar grains well grown within the lamellae of the DC coating and (**b**) α phase embedded in the γ matrix

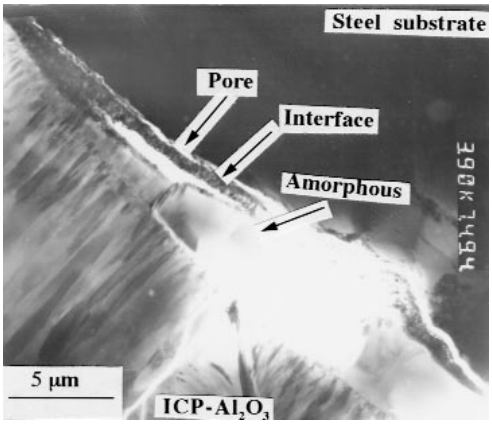

(a)

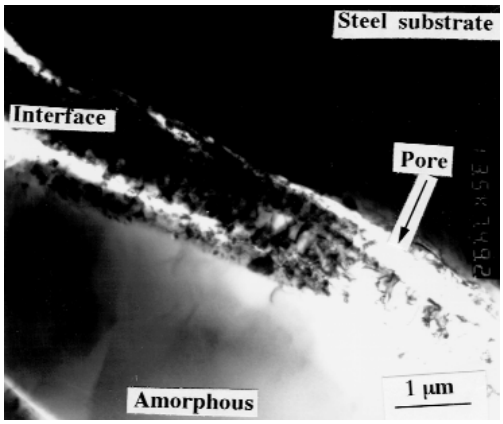

(b)

Fig. 11 TEM micrographs of the interfacial layer between the RF coating and the substrate: (**a**) morphology of the interfacial layer and (**b**) higher magnification of the amorphous region in (**a**)

was composed of a layer, about 1 μm thick, with different components across its thickness, as shown in Fig. 11(a). The interfacial layer was continuous and bordered by well-grown columnar grains at the coating side. In some locations of the interface, amorphous Al_2O_3 zones can be found between the columnar grains and the interfacial layer, as indicated in Figs. 11(a) and (b). With higher magnification, the interfacial layer was found to consist of three sublayers (regions), each of which has different morphologies and compositions, as annotated as regions A, B, and C in Fig. 12(a). Region A, close to the substrate, was composed of a series of crystals with different sizes and with the substrate material as a predominant material. Region C, on other hand, close to the edge of the interface layer, consisted of a mixture of equiaxed and platelike microcrystals with the coating material as the predominant material and with the γ phase as a predominant structure (Fig. 12b). Region B, however, was composed of an $AlFeO_3$ phase with the columnar grains growing perpendicular to the interface. The structures of all three regions were confirmed by SAED during TEM, and the compositions of all three regions were analyzed by the EDS qualitative microanalysis. Figures 12(c) and 12(d) show SAED patterns and EDS of region B. It is believed that the $AlFeO_3$ layer (region B) was formed due to the reaction between coating and substrate.

In addition to α and δ phases, TEM also shows γ phase existing in the RF coating, as shown in Fig. 13.

4. Discussion

4.1 Relation between the Coating Structure and Cooling Rates

Results from this work show that the phase composition and structure of the coatings depend on their deposition process. The DC coatings consist predominantly of γ plus α phases, while in the case of RF coatings, α and some δ phases are formed. So far the formation mechanism of α phase is not understood for either RF or DC plasma spraying. Previous work pointed out that the α phase was transformed from the γ phase during the coating formation due to the inherent annealing process by heating from subsequent deposited layers,[7] or that the α phase may be formed by incomplete melting of the starting powder.[9] Some work seems to indicate that the α phase remained unchanged from the original starting powder during coating formation.[10] Other work suggested that homogeneous nucleation of the solidification of liquid droplets at considerable undercooling results in the formation of the γ phase rather than

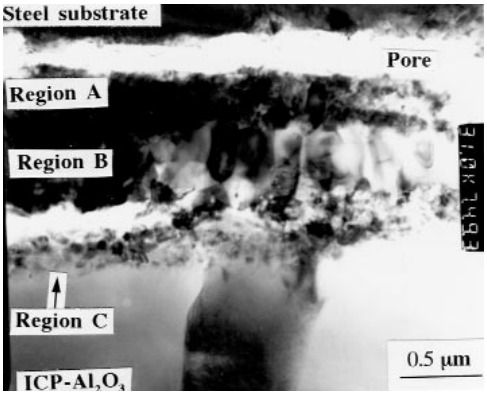

(a)

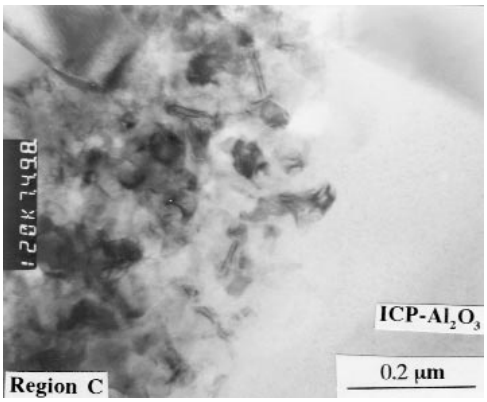

(b)

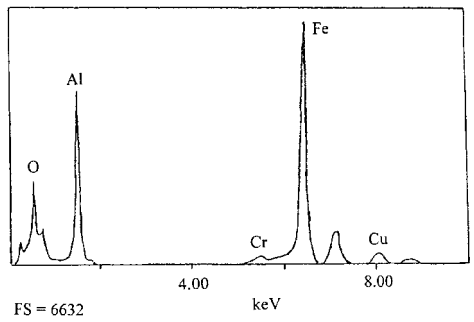

(c)

Fig. 12 TEM higher magnification of the interfacial layer in the RF coating: (**a**) interface layer consisting of three sublayers (regions), (**b**) morphology of region C, and (**c**) EDS of region B

α phase because of its lower critical free energy for nucleation.[11] Comparisons of phase structures between the RF and DC coatings in this work suggest that the α phase of the coating may be transformed from the γ phase during cooling and that the degree of transformation is affected by the cooling rates. The higher the cooling rate, the less the degree of the transformation, and thus a lower content of the α phase will exist in the coating. Compared to the RF spraying process, the DC spraying process results in higher cooling rates during the coating formation, because in this case, the substrate is attached to a rotating large disk and repeatedly traversed through the plasma jet and, thus, the heat from the substrate can be easily dispersed. As a consequence of the high cooling rates, the

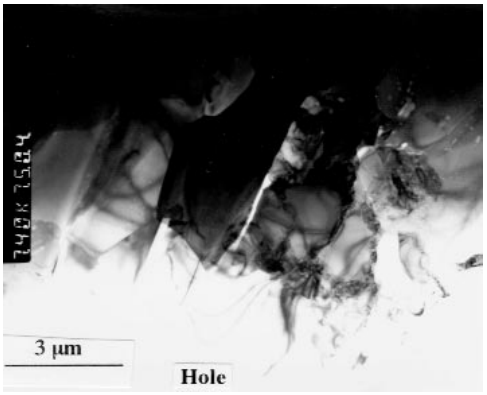

(a)

(b)

Fig. 13 TEM micrographs showing (**a**) morphology of γ phase grown in the α matrix and (**b**) SAED patterns of the γ region

metastable γ phase is retained at high temperatures and even the amorphous phase may be formed in the DC coating, because only a small amount of the α phase can be formed from the γ phase. In contrast, the transformation of the γ into the α phase is much more important in the RF process due to low cooling rates involved and, as a result, the α phase is found as the predominant phase in the coating.

It should be pointed out that the nature of lamellar structure of the coating is associated with the size and velocities of particles. Even large particles (≈100 μm) with lower velocities carry less momentum on impact on the substrate, compared with smaller particles (≈50 μm) with substantially higher velocities during the DC plasma spraying process. The lower momentum results in reduced contact areas between splats, giving rise to a more pronounced lamellar structure.

4.2 The Nature of the Coating-Substrate Interface

It has been found that the interface between the coating and substrate varies substantially with the coating process. Both the cooling rate and the momentum on impact of the particle on the substrate are responsible for the difference in the interfacial microstructure between the RF and DC spraying processes.

In the case of DC plasma spraying, the nature and formation mechanism of the amorphous interfacial layer containing both coating and substrate materials has been described in detail in a previous paper.[5] Because heat transfer from the first molten

droplets to the substrate may cause partial melting of the surface of the substrate, a thin layer of "mixed liquid" will be formed, which contains both the coating and the substrate materials. After spraying, this "mixed liquid" will form an amorphous layer between the coating and the substrate due to the quenching effect from the cold substrate. In some regions, it is possible that heat transfer from the first hot droplets impinging on the substrate may not be sufficient to melt the surface of the cold substrate. In this case, the "mixed liquid" will not be formed, and, thus, the interfacial layer cannot be detected; *i.e.*, only an amorphous Al_2O_3 is found in direct contact with the substrate, as shown in Fig. 8. In the case of RF plasma spraying, according to the EDS analysis, such a thin layer of the "mixed liquid" is also formed, because both coating and substrate materials have been detected. However, due to lower cooling rates and higher temperatures of the droplets involved in this process, the interfacial layer is wider and crystalline in nature. It is composed of three sublayers, each of which has different compositions and morphologies. These differences in composition and morphology across the interfacial layer are caused by the incomplete mixture of the "mixed liquid" due to low velocities and correspondingly low momentum of the particles on impact on the substrate. This incomplete "mixed liquid" results in the formation of region C, containing predominantly coating material, and region A, containing predominantly substrate material (Fig. 12a). When the composition and thermodynamic conditions of the "mixed liquid" meet the requirements for forming a chemical compound, a reaction layer (like region B) will be formed, as shown in Fig. 12(a). More work, however, is needed to completely understand the formation mechanism of this reaction layer.

5. Conclusions

Because RF and DC plasma spraying result in different particle heating and particle velocities, the morphology, phase structure, and fracture modes of the coatings vary substantially. The RF coatings show a pronounced lamellar microstructure and are composed predominantly of the α-Al_2O_3 phase, with delamination type fracture detected on the fracture surface. In contrast, the DC coatings consist predominantly of the metastable γ-Al_2O_3 as well as of amorphous phases, with a mixed fracture mode of the coating observed.

In spite of the limited interfacial diffusion detected by EMPA, TEM shows an interfacial layer existing at the interface between the coating and the substrate for both cases. For RF coatings, the interfacial layer is composed of three sublayers, each of which is different in composition and morphology. However, the interfacial layer for the DC coating consists primarily of an amorphous phase containing both coating and substrate materials, although in some regions a thick amorphous Al_2O_3 layer was in direct contact with the substrate.

Acknowledgments

This work has been supported through NSF/INT-9513702 and through the Deutsche Forschungsgemeinschaft Nu 59/6-1,2 and the Deutscher Akademischer Austauschdienst (DAAD).

References

1. K. Mailhot, F. Gitzhofer, and M.I. Boulos: *Proc. 1st UTSC.*, C.C. Berndt, ed., ASM International, Materials Park, OH, 1997.
2. L. Blanchi, A. Grimaud, F. Blein, P. Laucchese, and P. Fauchais: *J. Thermal Spray Technol.*, 1995, vol. 4 (1), pp. 59-66.
3. M.I. Boulos: *J. Thermal Spray Technol.*, 1992, vol. 1 (1), pp. 33–40.
4. W.D. Swank, J.R. Fincke, and D.C. Haggard: *J. Thermal Spray Technol.*, 1993, vol. 2 (3), pp. 243-49.
5. H.C. Chen, J. Heberlein, and E. Pfender: *Thin Solid Films*, 1997, vol. 301, pp. 105-14.
6. P.D. Harmsworth and R. Stevens: *J. Mater. Sci.*, 1992, vol. 27, pp. 616-24.
7. J.M. Guilemany, J. Nutting, and M.J. Dougan: *J. Thermal Spray Technol.*, 1997, vol. 6 (4), pp. 425-29.
8. H.C. Chen and E. Pfender: *Thin Solid Films*, 1996, vol. 280, pp. 188-98.
9. D.A.J. Ramm, T.W. Clyne, A.J. Strugeon, and S. Dunkerton: in *Thermal Spray Industrial Applications*, C.C. Berndt and S. Sampath, eds., ASM International, Materials Park, OH, 1994, pp. 239-44.
10. B. Dzur and G. Nutsch: *Proc. 12th Int. Conf. on Gas Discharges and Their Applications*, Greifswald, Germany, 1997, pp. 342-46.
11. R. McPherson: *J. Mater. Sci.*, 1973, vol. 8 (6), pp. 851-58.